Philosophical Magazine

ISSN: 0031-8086 (Print) (Online) Journal homepage: www.tandfonline.com/journals/tphm19

Vacancy condensation and void formation in duplex oxide scales on alloys

M. G. C. Cox, B. McEnaney & V. D. Scott

To cite this article: M. G. C. Cox, B. McEnaney & V. D. Scott (1973) Vacancy condensation and void formation in duplex oxide scales on alloys, Philosophical Magazine, 28:2, 309-319, DOI: 10.1080/14786437308217455

To link to this article: https://doi.org/10.1080/14786437308217455

Vacancy condensation and void formation in duplex oxide scales on alloys

By M. G. C. Cox, B. McEnaney and V. D. Scott
School of Materials Science, University of Bath, U.K.

[Received 10 March 1973]

Abstract

The growth of duplex scales on iron–chromium alloys oxidised at 600°C in CO_2–1% CO gas is accompanied by the formation in the inner oxide layer of regularly-spaced lamellar voids parallel to the metal–oxide interface. It is proposed that these voids form at the metal–oxide interface by periodic condensation of vacancies which have been injected into the metal by the oxidation process. From lamellar void spacings, the vacancy fraction in the metal at condensation is estimated to be 6×10^{-3} and the energy to precipitate the first vacancy, E_v, is $\sim 2{\cdot}7 \times 10^{-19}$ J. From consideration of surface energy changes accompanying lamellar void formation, an average value of $E_v = 1{\cdot}3 \times 10^{-19}$ J is estimated. The effects of chromium content in the metal and specimen geometry on lamellar void spacings are consistent with the proposed mechanism. The presence of filamentary microcrystals of oxide in the lamellar voids suggests that the inner oxide grows by gas phase transport of the oxidant to the metal surface.

§ 1. Introduction

Although considerable information has been obtained over a number of years on the formation and behaviour of vacancies in materials subjected to irradiation, quenching or mechanical treatment, the part played by vacancies in oxidation reactions has received relatively little attention. Experimental verification of the generation of vacancies during oxidation has been provided by observations on dislocation loop growth in metal foils oxidized in the electron microscope (Hales, Dobson and Smallman 1968), while the frequent occurrence of void dispersions in oxide scales has been attributed (e.g. Mindel and Pollack 1969) to precipitation of vacancies generated during the oxidation process. Clearly, vacancies and voids have a significant role in oxidation reactions. For example, diffusion of ions in oxide and metal may be sensitive to vacancy concentrations, while voids in the scale may block diffusion paths (Evans 1948), or may allow penetration of the oxidising gas to the metal (Dravnieks and McDonald 1948, Mrowec 1967) and may impart mechanical weakness to the oxide layer (Tylecote and Mitchell 1960).

This paper considers diffusion of vacancies and their role in void formation within duplex oxide scales formed on iron-chromium alloys heated in CO_2–1% CO gas at 600°C ; it follows an earlier paper (Cox, McEnaney and

Scott 1972) on cation diffusion and segregation of elements in duplex oxide scales. A model for vacancy condensation at the metal–oxide interface is presented which accords with experimental data. Evidence for inward transport of gaseous oxidant through the inner oxide is also described.

§ 2. Experimental details

Details of oxidation experiments and techniques used for examination of the oxidation products have been given previously (Cox *et al.* 1972). Studies have been carried out on sheet specimens (1 mm thickness) prepared from binary iron alloys containing 5, 9, 12, 15 and 20% chromium ; in addition, specimens of the 9% chromium alloy of thickness 0·5 and 2·15 mm have been investigated.

In current work, in addition to scanning and transmission electron microscopy, electron diffraction and X-ray diffraction techniques referred to in the earlier paper, a combined electron microscope/microanalyser (EMMA 4) has been used to analyse oxidation products.

Fig. 1

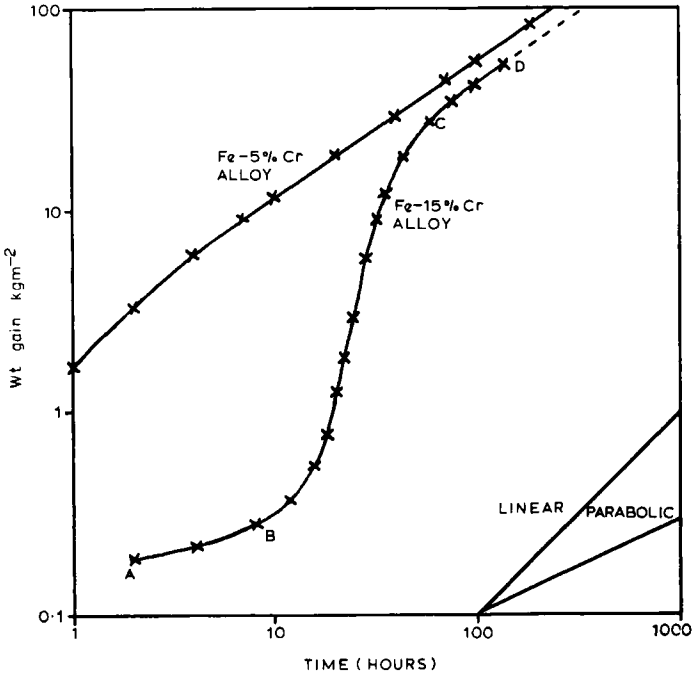

Oxidation of 5% and 15% chromium alloys at 600°C in CO_2-based gas. Plots of log (wt. gain) versus log (time) ; lines with slopes of unity and one-half, corresponding to linear and parabolic growth kinetics, are shown in the lower right-hand corner.

§ 3. Experimental results

3.1. *Kinetic experiments*

Kinetic data (weight gain versus time) for the 5 and 15% chromium alloys are illustrated in fig. 1. The curve for the 15% chromium alloy may be divided into three regions, an initial oxidation or primary stage (AB), a secondary stage with parabolic kinetics (CD) and a transitional region (BC); the length of the primary oxidation stage for this alloy differed from specimen to specimen and one sample had not entered fully the secondary stage after 150 hours oxidation. The primary stage was not detectable in the 5% chromium alloy, the metal undergoing parabolic oxidation kinetics almost from the start of the experiment. The oxidation of the 20% chromium alloy was similar to the 15% chromium alloy with a distinct primary stage, while the oxidation kinetics of the 9% and 12% chromium alloys more closely resembled those exhibited by 5% chromium alloy. The parabolic rate constant for each composition is listed in table 1 and it can be seen to be effectively independent of chromium content.

Table 1. Data for oxidation of iron–chromium alloys in CO_2-based gas at 600°C

Cr in alloy (wt. %)	Primary oxidation stage observed	Parabolic rate constant for secondary stage	Spinel formula for inner oxide†
		$kg^2\ m^{-4}\ sec^{-1} \times 10^8$ ($\pm 0{\cdot}3$)	$Fe(Fe_xCr_{2-x})O_4$ x ($\pm 0{\cdot}1$)
5	No	1·2	1·7
9	No	0·9	1·4
12	No	0·7	1·2
15	Yes	0·8	1·0
20	Yes	1·2	0·8

† Outer oxide magnetite, Fe_3O_4, in every case.

3.2. *Microstructural results*

Reflection electron diffraction patterns from 15 and 20% chromium alloys examined after the primary oxidation stage indicated that the surface layer consisted of a mixture of rhombohedral oxide and spinel oxide. Selected area electron diffraction on chemically stripped films showed that the rhombohedral oxide was thin and covered the entire surface, apart from isolated regions where thicker oxide with the spinel structure had grown. As oxidation proceeded, the extent of the spinel growth increased until it covered the surface; this is illustrated in a series of scanning electron micrographs, figs. 2 (*a*)–(*c*). The lateral growth of spinel can be related to the transitional period between the primary and

Fig. 2

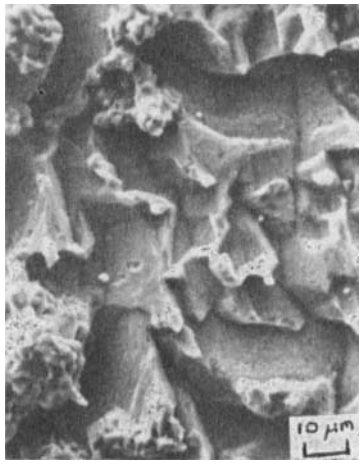

(*a*)

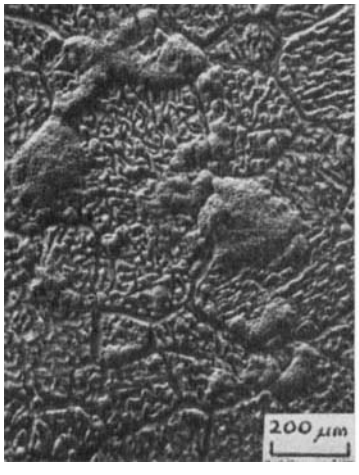

(*b*)

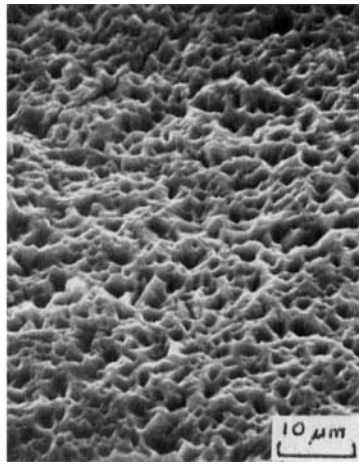

(*c*)

Oxidised surface of 15% chromium alloy showing lateral growth of spinel oxide. Scanning electron micrographs.

secondary oxidation stages. A selection of optical micrographs taken from polished sections through specimens shows the development of patchy oxide on 15% chromium alloy while in the transitional stage, fig. 3 (*a*), and the formation of a continuous, thick oxide scale when the samples were in the secondary parabolic stage, figs. 3 (*b*)–(*c*) from 9% chromium alloy. The thick spinel oxide consists of two layers of approximately equal thickness, and is a characteristic feature of the alloys oxidized under these conditions. The oxide–oxide interface is located in the plane of the original metal surface, fig. 3 (*a*). Diffraction techniques combined with electron-probe microanalysis identified the outer scale as magnetite,

Fig. 3

(*a*)

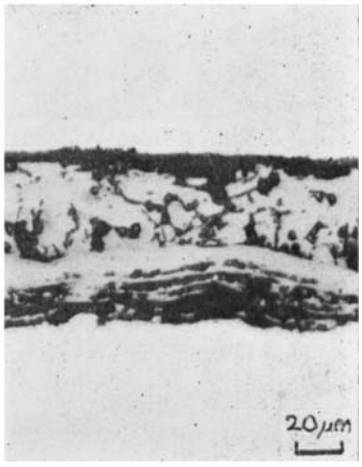

(*b*) (*c*)

Sections through oxidized alloys : optical micrographs. (*a*) 15% chromium alloy after 94 hour exposure, showing patchy growth ; note location of oxide-oxide interface at original metal surface. (*b*) 9% chromium alloy after 20 hour exposure, showing duplex oxide scale and lamellar voids. (*c*) 9% chromium alloy after 140 hour exposure, showing a well-developed series of lamellar voids ; note the voids in outer layer concentrated at the oxide–oxide interface.

Fe_3O_4, and the inner layer as a mixed spinel $(Fe, Cr)_3O_4$; the chromium content of the inner oxide increases with increasing chromium content of the alloy, table 1.

The outer layer (magnetite) consists of columnar crystals which contain voids, the void fraction decreasing with distance from the oxide–oxide interface. Voids are also present in the inner layer and fig. 3 (*b*) shows

that many of these are arranged in lamellar distributions parallel to and some 6 μm from the oxide–oxide interface. Following more prolonged exposure, a succession of lamellar distributions of voids has developed, fig. 3 (*c*), with separations of ~ 3 μm ; the lamellar void spacings found for the different alloys are given in table 2. It can be seen that distances between successive lamellar voids are independent of alloy composition, although the distance from the oxide–oxide interface to the first visible lamellar void increases with chromium content.

Table 2. Effect of specimen thickness and chromium content on lamellar void spacings in the inner oxide

Cr in alloy (wt. %)	Specimen thickness (mm)	A† (μm)	B‡ (μm)
5	1·0	3 (±1)	3
9	1·0	6 (±2)	3
9	2·1	12 (±3)	6
9	0·5	6 (±2)	<2
12	1·0	10 (±3)	3
15	1·0	13 (±4)	3
20	1·0	>20	—

† Distance from oxide–oxide interface to first visible lamellar void.
‡ Distance between successive lamellar voids.

Void distributions in the inner layer were found to be affected by the rate of cooling of the specimen from the oxidation temperature. A large lamellar void at the oxide–metal interface was usually found upon slow cooling ($\sim 10^{-2}$ deg K sec^{-1}) but rarely observed after rapid cooling (~ 1 deg K sec^{-1}) from the oxidation temperature.

Fig. 4

Filamentary microcrystals of spinel oxide extracted from inner oxide layer. Electron micrograph.

The duplex oxide was hard, brittle and readily detached, cleavage occurring along the lamellar voids to reveal a brown, friable, underlying oxide which 'ghosted' the grain structure of the metal. Between the layers of compact oxide forming the inner oxide scale, filamentary crystals < 1000 Å in diameter and several μm in length were found, fig. 4. The filaments were found to be spinel with [111] parallel to the axis and to have the same chemical composition as the bulk of the inner oxide layer (see table 1).

§ 4. Discussion

The kinetics of oxidation of 15% and 20% iron–chromium alloys at 600°C can be conveniently divided into three periods: a relatively slow oxidation (the primary stage) followed by a transitional stage and then a faster, parabolic rate of oxide growth (the secondary stage). The duration of the primary stage was found to be sensitive to chromium content, surface preparation and crystal orientation of the substrate metal. The primary stage could not be detected in alloys containing up to 12% chromium, such alloys following a parabolic rate law almost from the start of the experiment (table 1). The 15% and 20% chromium alloys, however, exhibited primary oxidation behaviour for periods of up to hundreds of hours, although the duration was not reproducible from specimen to specimen for either composition. A detailed treatment of factors affecting the primary oxidation stage will be discussed in a later publication; this paper is concerned particularly with the role of vacancies in the formation of duplex oxide scale during the secondary stage.

4.1. *Formation of duplex scales*

A metallographic section through the oxide scale in the transitional stage, fig. 3 (*a*), clearly demonstrates that the interface between the two oxide layers is located at the original metal surface. This indicates that the outer layer grows by the movement of cations outwards and the inner layer by inward migration of an oxygen-containing species, in agreement with earlier findings (Cox *et al.* 1972). The concentration of chromium in the inner layer, a mixed spinel of composition $(Fe, Cr)_3O_4$, has been explained using crystal field theory to deduce relative diffusion rates for transition metal cations through close-packed oxides. It was shown that Fe^{3+} diffuses much more readily than Cr^{3+} to form the outer layer of Fe_3O_4. Cation diffusion through the outer oxide may be deduced to be rate-controlling and, since the rate of cation diffusion through the outer magnetite layer would be independent of chromium content of the alloy, the compositions studied exhibited the same parabolic oxidation rate.

As the outer oxide is formed, vacancies are injected into the metal. Direct evidence on vacancy mobility in iron-chromium alloys at 600°C is not available, but a high mobility may be inferred using comparative data on vacancy migration energies; $E_m = 0{\cdot}76$ eV, 1·1 eV and 1·5 eV for

iron, copper and nickel respectively (Smallman 1970). The vacancy jump frequency, ω, may be written $\omega = z\nu \exp[-E_m/kT]$, where z is the coordination number and ν is the atomic vibration frequency. For iron at 600°C, $\omega = 3{\cdot}2 \times 10^9\ \mathrm{sec}^{-1}$. This value is of the same order of magnitude as jump frequencies calculated for copper at 1000°C ($4{\cdot}1 \times 10^9\ \mathrm{sec}^{-1}$) and nickel at 1100°C ($3{\cdot}4 \times 10^8\ \mathrm{sec}^{-1}$), at which temperatures vacancies are known to be mobile in these metals (Appleby and Tylecote 1970, Hales and Hill 1972). Hence it would be expected that diffusion of vacancies would readily occur in the lattice of the iron–chromium alloy, further enhanced by a grain-boundary contribution at the oxidation temperature. Initially these vacancies will be retained in solution, until their concentration reaches a critical level when they may condense into voids at suitable precipitation sites. The appearance of voids aligned parallel to the metal–oxide interface indicates that this is the preferred site in the iron–chromium system. There is evidence that the metal can retain a high concentration of vacancies, since samples slowly cooled in the oxidation furnace were usually found to contain a void at the metal–oxide interface whereas rapidly cooled specimens did not. The likelihood of stress contributing to void formation may be discounted because rapid cooling would favour the formation of an interfacial void as the mode of stress relief.

It follows that, after vacancy condensation has occurred, the vacancy excess in the metal would have to increase to the critical fraction before further vacancy rejection can take place. This would necessitate further oxide formation, by which time the metal–oxide interface would have advanced a discrete distance into the metal. Thus the periodic character of lamellar voids may be explained.

The presence of voids in the inner layer indicates that growth of inner oxide may not take up completely the space created by vacancy condensation. Such a situation can arise when the rate of growth of the inner layer becomes less than the rate of vacancy injection into the metal. As the oxide scale thickens the rate of growth of the inner layer becomes dependent upon the rate of supply of gaseous oxidant through pores and channels in the oxide scale. It is apparent that penetration of gaseous oxidant occurs readily in the early stages of oxidation, since the distance between the oxide–oxide interface (the original metal surface) and the first-formed lamellar void is usually greater than interlamellar void spacings, table 2. In the later stages of oxidation, pores and channels in the outer layer become blocked by growth of oxide within them, as evidenced by the location and shape of voids close to the oxide–oxide interface in that layer, fig. 3 (*c*). In accord with this view, the occurrence of oxide crystals of filamentary habit in lamellar voids within the inner oxide is indicative of a growth process limited by gas phase diffusion. Lamellar voids are not observed in the 20% chromium alloy, which suggests that the growth rate of the inner oxide is not significantly reduced in this case. The effect may be attributed to the high affinity of chromium

for oxygen, which enables the 20% chromium alloy to oxidize more readily than lower-chromium alloys in low partial pressures of oxidant. This explanation would also account for the effect of chromium content of the metal on the location of the first-formed lamellar voids, table 2.

The presence of voids in the inner oxide scale does not significantly interfere with the rate of outward movement of cations since the parabolic rate constant is independent of the void structure in scales, table 1. This may be attributed to the presence of the filamentary crystals which bridge voids and provide a diffusion path for cations. The high surface to volume ratio ($> 4 \times 10^5$) of the filamentary crystals suggests that surface diffusion may be the mode of transport of cations (Tagati 1957). This view is supported by the high level of chromium found in these crystals, i.e. lattice diffusion of chromium is difficult in spinel oxides (Cox *et al.* 1972), implying that an alternative mode of transport is involved.

4.2. *Vacancy condensation model*

The critical fraction of vacancies in the metal required for condensation to take place at the metal–oxide interface may be estimated from the interlamellar void spacing. Consider a piece of metal sheet, thickness t_1 and area A, covered with a layer of oxide containing lamellar voids of spacing t_2. Since oxidation occurs on both surfaces, the vacancy fraction injected into the metal is given by $2t_2A/t_1A = 2t_2/t_1$, ($t_2 \ll t_1$), assuming no plastic deformation occurs at the oxidation temperature.

The use of typical experimental values from the present study of $t_1 = 10^{-3}$ m and $t_2 = 3 \times 10^{-6}$ m, table 2, gives a vacancy fraction of 6×10^{-3}. This value is much greater than the equilibrium vacancy fraction of $\sim 10^{-12}$ calculated using the quoted value for energy of vacancy formation of 2·13 eV for iron (Smallman 1970). The excess vacancy fraction is higher than values reported on materials quenched from temperatures close to the melting point ($\sim 10^{-4}$), but is of the same order of magnitude as excess vacancy concentrations produced by irradiation ($\sim 10^{-3}$; Cooper, Koehler and Marx 1955). Quantitative data on vacancy concentrations caused by oxidation treatment are not readily available, although a value $\sim 10^{-2}$ can be inferred from a study on Fe–Cr–Al–Y alloys. (Tien and Rand 1972).

The minimum vacancy concentration, c, for vacancy precipitation to occur in the manner proposed can be expressed as $C = C_E \cdot \exp[E_v/kT]$, where C_E is the equilibrium vacancy concentration and E_v is the maximum energy required to induce a vacancy to condense at the interface. Using the above values for C and C_E and taking $T = 873$ K and $k = 1{\cdot}38 \times 10^{-23}$ JK^{-1} gives $E_v = 2{\cdot}7 \times 10^{-19}$ J.

An alternative approach to this problem is to consider the creation of a new internal surface by separation of the oxide–metal interface. The surface free energy change per unit area, ΔF_s, may then be written $\Delta F_s = (\gamma_m + \gamma_o - \gamma_{mo})$, where γ_m, γ_o, γ_{mo} are the specific surface free energies

for metal–vapour, oxide–vapour and metal–oxide interfaces respectively. The cross-sectional area of a vacancy is given approximately by d^2, where d is the atomic spacing ($=2{\cdot}5\times10^{-10}$ m), and hence the average energy to induce each vacancy to condense at the interface is $E_v \approx (\gamma_m+\gamma_o-\gamma_{mo})d^2$. Taking $\gamma_m = 1{\cdot}4$ Jm^{-2} (Jones 1971), and reasonable estimates for $\gamma_{mo}\approx 0{\cdot}4$ Jm^{-2} (Turpin and Elliot 1966) and $\gamma_o \approx 1{\cdot}0$ Jm^{-2} (Kelly 1966) gives $(\gamma_m+\gamma_o-\gamma_{mo})\approx 2$ Jm^{-2}, and $E_v \approx 1{\cdot}3\times10^{-19}$ J. This is the average energy per vacancy to form an extended two-dimensional void. Despite the approximations involved in both calculations, the values of E_v estimated by the two methods are in satisfactory agreement. In principle E_v calculated from the vacancy condensation model is expected to be higher, since more energy would be required to precipitate the first vacancy than to enlarge the cluster by subsequent vacancy absorption.

According to the model, with thicker specimens more vacancies would have to be produced to reach the critical level, and therefore a correspondingly thicker oxide film would have to be formed on the metal surface. Indeed if the above assumptions remain valid, a direct relationship between specimen thickness and interlamellar spacing would be expected. This conclusion is qualitatively supported by the changes in interlamellar spacings observed in the three specimens of iron–9% chromium alloy of different thicknesses, table 2. It also follows that at intersecting surfaces a higher local vacancy flux would be injected into the metal than at a planar surface, leading to a greater incidence of voids at specimen corners as observed by other workers (Mrowec 1967).

The possible contribution of voids to mechanical weakness of the oxide scale is revealed by ready separation of the layer along lamellar voids under low applied stresses. It is possible that in practical applications of such alloys detachment of oxide scale from the metal may occur as a result of stresses imposed, for example by thermal cycling, with consequent reduction of the protective character of the scale. If, therefore, the void distribution could be suitably modified, an improvement in adhesion of the oxide scale to the metal might be achieved. It also follows that, since voids are associated with vacancy condensation, additions to the alloy may be beneficial if they (*a*) create sites remote from the interface at which vacancy condensation can occur, (*b*) promote the growth of inner oxide to fill space created by vacancies or (*c*) stabilize the vacancies in solution before they condense. It would be useful to test the argument by adding to the metal solute atoms which have a high vacancy-binding energy.

Acknowledgments

The authors wish to thank Dr. W. H. Whitlow for helpful discussions, Dr. G. W. Lorimer for the use of EMMA 4 and the CEGB for permission to publish this paper.

References

Appleby, W. K., and Tylecote, R. F., 1970, *Corros. Sci.*, **10,** 325.
Cooper, H. G., Koehler, J. S., and Marx, J. W., 1955, *Phys. Rev.*, **97,** 599.
Cox, M. G. C., McEnaney, B., and Scott, V. D., 1972, *Phil. Mag.*, **26,** 839.
Dravnieks, A., and McDonald, H. J., 1948, *J. Electrochem. Soc.*, **94,** 139.
Evans, U. R., 1948, *Corrosion*, **4,** 149.
Hales, R., Dobson, P. S., and Smallman, R. E., 1968, *Metal Sci. J.*, **2,** 224.
Hales, R., and Hill, A. C., 1972, *Corros. Sci.*, **12,** 843.
Jones, H., 1971, *Metal Sci. J.*, **5,** 15.
Kelly, A., 1966, *Strong Solids* (Oxford University Press).
Mindel, M. J., and Pollack, S. R., 1969, *J. Phys. Chem. Solids*, **30,** 993.
Mrowec, S., 1967, *Corros. Sci.*, **7,** 563.
Smallman, R. E., 1970, *Modern Physical Metallurgy* (Butterworths).
Turpin, M. L., and Elliot, J. F., 1966, *J. Iron Steel Inst.*, **204,** 217.
Tagati, R., 1957, *J. Phys. Soc. Japan*, **12,** 1212.
Tien, J. K., and Rand, F. S., 1972, *Scripta Metall.*, **6,** 55.
Tylecote, R. F., and Mitchell, T. E., 1960, *J. Iron Steel Inst.*, **196,** 445.